PRIMA

Small or medium-scale focused research project

SEVENTH FRAMEWORK PROGRAMME

THEME FP7-ICT-2009-4

INFORMATION SOCIETY TECHNOLOGIES

Deliverable 1.2 – Report on the evaluation of the potential broadband device performance based on scattering and near-field effects

Dissemination level: Public

Contract no.:	248154
Project acronym:	PRIMA
Project full title:	Plasmon Resonance for IMproving the Absorption of solar cells
Project website:	http://www.prima-ict.eu

Coordinator contact details: Barry Rand (rand@imec.be)
IMEC

Kapeldreef 75
B-3001 Heverlee
Belgium

Table of Contents:

1 Introduction

This report is divided into two distinct sections; the first considers theoretical contributions to the evaluation of plasmonic GaAs solar cells, while the second section outlines some experimental work towards the broadband performance enhancement of Si solar cells.
In order to theoretically evaluate the broadband performance of plasmonic solar cell devices both optical and electrical calculations are required. The optical part requires the solution of Maxwell's equations to gain an understanding of the absorption profile in the solar cell, while the electrical calculation relates the absorption to the electrical properties and efficiency of the solar cell. To date no one has completed both of these calculations in the same model, instead relying on the assumption that an increase in the absorption automatically translates to an increase in the device efficiency. In the first section of this document we report on the design and realisation of a solar cell simulation which incorporates both the optical and electrical calculations in a single model. Furthermore we will show how this model has been used to optimise the design of plasmonic nanoparticle arrays for broadband enhancements in device performance.
The second section of the report is concerned with the experimental realisation of spectrally broadband enhancements to the optical response of Si based solar cells. We will demonstrate the use of Ag nanodisk structures to enhance light trapping in a Si wafer, thereby increasing the amount of light available for absorption. In addition we will present the use of Au disk-on-film structures for application to the rear surface of a solar cell. These structures have been designed to provide broadband scattering of light which has not been absorbed on the first pass back into the solar cell.

2 Theoretical work

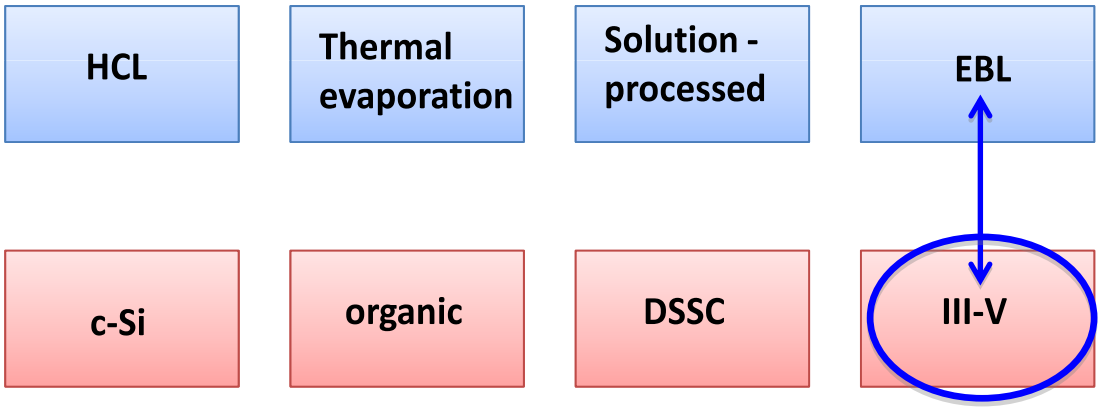

This section considers theoretical work towards III-V plasmonic solar cells to be fabricated using electron beam lithography.

2.1 Simulation theory

Our motivation is to develop a robust optical and electronic calculation for plasmonic solar cells in both the frequency and all spatial domains. By employing periodic nanoparticle arrays, we are able to consider only one period and utilise periodic boundaries to accurately represent a complete structure. This approach is applicable for both the optical and electronic calculations in our model and significantly decreases the computation time.
As stated in Deliverable 1.1 there are a number of numerical solution methods which can be employed to examine the optical responses of plasmonic solar cells under solar illumination, e.g., finite difference time domain (FDTD), finite element method (FEM) and Greens-based methods. However, the

electronic part of the calculation must take account of the carrier diffusion and drift characteristics in 3D, which dictates the use of FEM calculations in the form of commercial software, COMSOL Multiphysics. The modular nature of COMSOL Multiphysics allows us to perform the optical calculation first and use the results as the initial conditions for the electrical calculation. This part is composed of three stages; two convection-diffusion stages for describing the carrier diffusion due to carrier mobility and carrier drift effects arising from the build-in electric field, followed by a Poisson solver to connect the electrostatic potential with the charge distribution in the device.

2.2 Simulation results

Initially a comparison between our calculation and the results of experiments on GaAs-based solar cells from the literature will first be given to verify the validity of our 3D simulation. The model will then be used to investigate GaAs-based plasmonic solar cells with periodic arrays of silver nanoparticles decorating the AlGaAs window layer. The changes to the optical and electronic response of the solar cell due to the introduction of plasmonic nanostructures will be discussed and verified.

2.2.1 Model verification

We first use our model to simulate GaAs solar cells reported by Tobin et al [1-3]; the solar cell structures consist of antireflection coatings (ARCs) composed of MgF_2 (100 nm) and ZnS (50 nm) layers, a p-$Al_{0.8}Ga_{0.2}As$ window layer (30 nm), a p-GaAs emitter (500 nm), a n-GaAs base (3500 nm), and a n-$Al_{0.3}Ga_{0.7}As$ back surface field (BSF) layer (500 nm). Using our model, we calculated current densities, external quantum efficiency (EQE), internal quantum efficiency (IQE), device reflection (R), and current-voltage (IV) characteristics as displayed in Fig. 1. Standard solar incidence spectrum (AM1.5G) is used as the source of the model. The calculated performance parameters, including short-circuit current density (J_{sc}), open-circuit voltage (V_{oc}), fill factor (FF), and light-conversion efficiency (η) are listed in Fig. 1(c). The values reported from the experiment are J_{sc} = 27.89 mA/cm^2, V_{oc} = 1.029 V, FF = 86.43%, and η = 24.8%. Our simulation results are very close to the experimental reports shown in Figs. (d) and (e) [1-3]; the slight difference is due to the fact that we could not obtain all of the experimental parameters accurately.

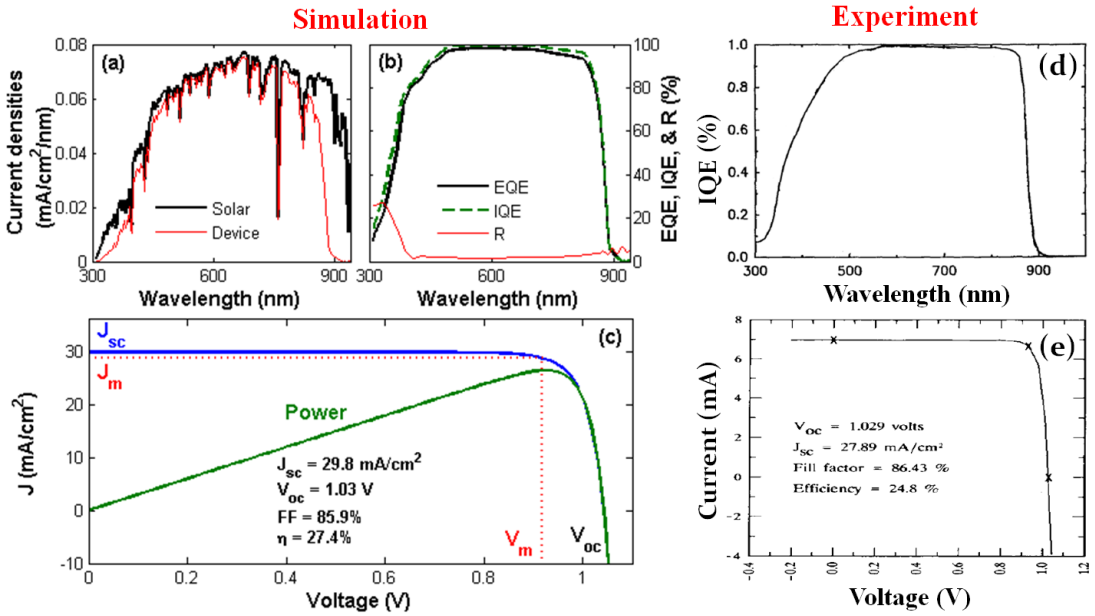

Fig. 1 (a) Calculated current densities given by the solar spectrum and that collected by the device, (b) calculated EQE, IQE and *R* spectra, and (c) IV characteristics calculated from our model. Experimental EQE response (d) and IV curve (e) [1-3].

Next we turn our attention to the simulation of an optically-thin GaAs solar cell [4]. The device is composed of a p-$Al_{0.8}Ga_{0.2}As$ window layer (30 nm), a p-GaAs emitter (50 nm), a n-GaAs base (150 nm), and a n-$Al_{0.2}Ga_{0.8}As$ BSF layer (500 nm). According to the results shown in Ref. [4], the device has a low V_{oc} and a small FF, which are believed to be the results of a high bulk recombination rate and a large series resistance. Therefore, to better match the experiment, certain device parameters, including device series resistance, surface recombination rates and carrier lifetimes are carefully selected. Our simulation results are shown in Fig. 2, where the current densities, EQE, IQE, *R*, and IV curves are all plotted. The graphs clearly show that the performance of the thin GaAs solar cell is significantly degraded when compared to the case shown in Fig. 1. Once again, however, the results of our simulation agree well with those of the experiment [4] [see Figs. (d) and (e)], where the performance parameters are J_{sc} = 11.0 mA/cm^2, V_{oc} = 0.73 V, FF = 55.0%, and η = 4.7%.

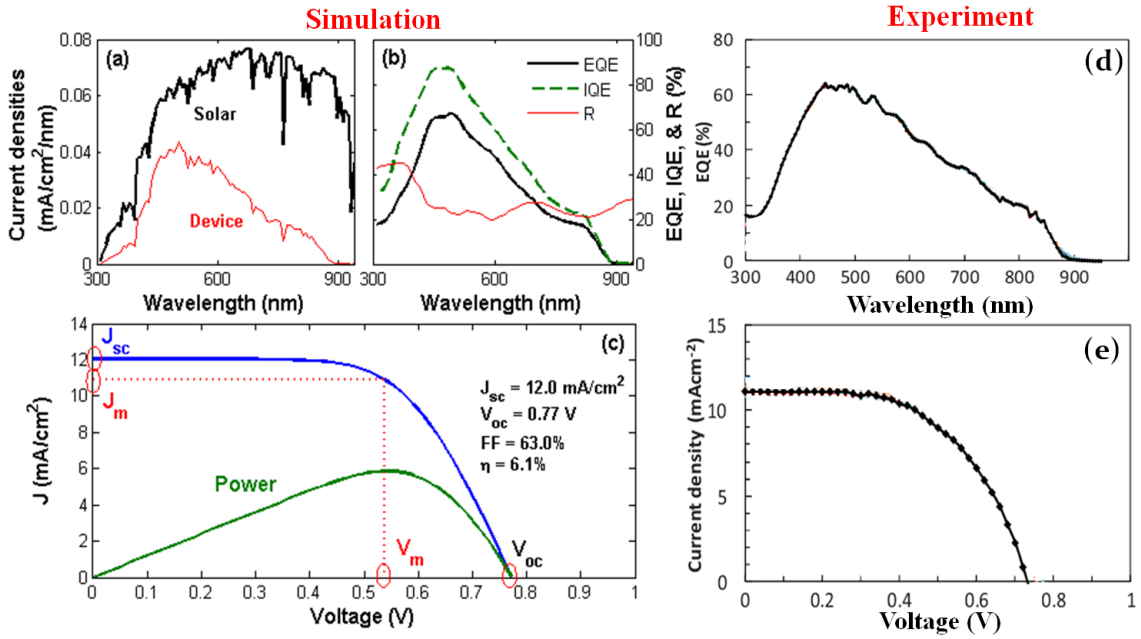

Fig. 2 (a) Current densities from solar and collected by the device, (b) EQE, IQE and *R* spectra, and (c) IV characteristics calculated from our model. Experimental EQE response (d) and IV curve (e) [4].

Good agreement has also been achieved between our model and PC1D (results are not given here), which is a popular software (working in 1D only) used in industry to assist solar cell design. However, PC1D cannot be used to simulate those devices with a more complex configuration, e.g., with plasmonic nanostructures, and carrier generation is not treated comprehensively. Having satisfactorily simulated conventional and thin-film III-V solar cells, hence verifying the validity of our 3D model, the application of plasmonic nanoparticles will now be considered. It is particularly relevant to introduce plasmonics in the case of thin-film solar cells, since they exhibit comparatively poor performance.

2.2.2 Plasmonic solar cell design

In this section, we will present a plasmonic design for the thin-film GaAs solar cells previously discussed. An optimal design will be achieved by properly choosing the particle size as well as the particle separation through a systematic 3D simulation.

As shown in Fig. 2 the surface reflection of the device is strong due to the absence of ARCs. However, this loss can be significantly reduced with the incorporation of properly designed plasmonic nanostructures. Figs. 3 and 4 show how the plasmonic design can be used to control the EQE and reflection of the thin-film GaAs solar cell by adjusting the particle dimension and particle array period. With the presence of plasmonic structures the device absorption can be enhanced over a broadband spectral region and correspondingly the EQE performance can be improved as shown in Figs. 3(a) and 4(a). However, according to our calculation, the dependence of the solar cell performance upon the metallic particle configuration is complex and therefore optimal design has to be found so that the best light-collection capability can be achieved. We calculated the dependence of J_{sc} on particle radius R_M and particle array period Λ, respectively (shown in the insets of figs. 3 (a) and 4 (a)). The results indicate that the particle arrays with R_M = 80 nm and Λ = 400 nm, provide the best trade-off between scattering and metallic absorption and hence the maximum obtainable J_{sc}.

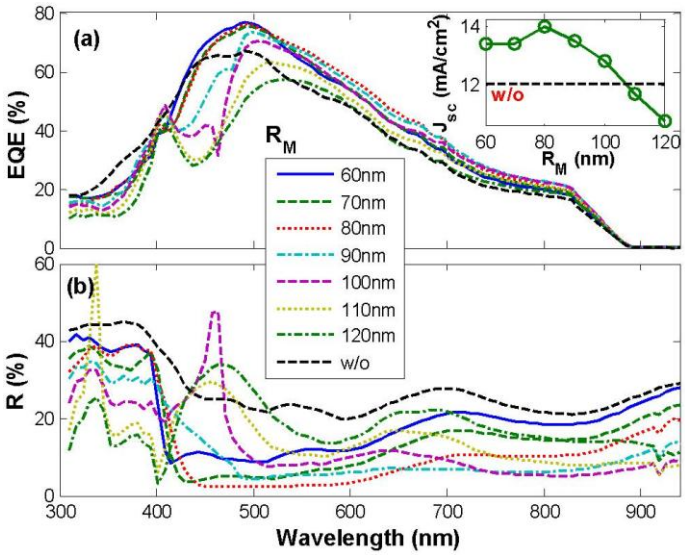

Fig. 3 (a) EQE and (b) R spectra of the plasmonic solar cells for different particle radii, i.e., R_M = 60, 70, 80, 90, 100, 110, and 120 nm, respectively. The period of the square particle array is Λ = 400 nm. The results for the solar cells without plasmonic effect are given as well for comparison. The dependence of J_{sc} on R_M is inserted into Fig. 3(a) where optimal particle dimension can be determined.

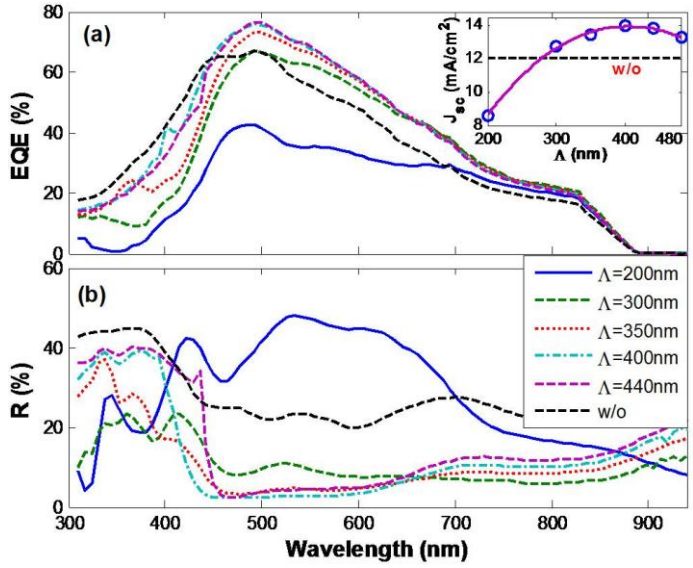

Fig. 4 (a) EQE and (b) R spectra of the plasmonic solar cells with Λ = 200, 300, 350, 400, and 440 nm, respectively. R_M = 80 nm determined from Fig. 3 is used in this calculation. The results for the solar cells without plasmonic effect are given as well for comparison. The dependence of J_{sc} on Λ is given in the inset of Fig. 4(a).

Following the calculation of EQE and reflectivity of the plasmonic solar cell, the key performance parameters J_{sc}, V_{oc}, P_{max}, FF, and η, (which can be extracted from the IV curve by taking account of both photocurrent and dark current) were calculated. The value of J_{sc} = 14 mA/cm^2 was computed according to the EQE response obtained previously, while the dark current can be found by performing an electric transport calculation with forward bias applied to the device. The calculated IV curves for both with and without the proposed plasmonic designs are plotted in Fig. 5, where the corresponding output power densities are also given in order to find the condition with a maximal electrical output. The improvement of IV characteristics due to plasmonic design is apparent from the figure and the performance parameters extracted from Fig. 5 are listed in Table 1. The incorporation of plasmonic nanostructures leads to an increase in J_{sc} of over 16% and reduces the device series resistance. As a result P_{max} and FF are improved by 38.6% and 18.3%, respectively. Therefore, the light-conversion efficiency is finally found to be increased by 39.3% (from 6.1% to 8.5%). These results verify that the systematic design of plasmonic nanostructures can be very useful for the realization of broadband efficiency enhancements.

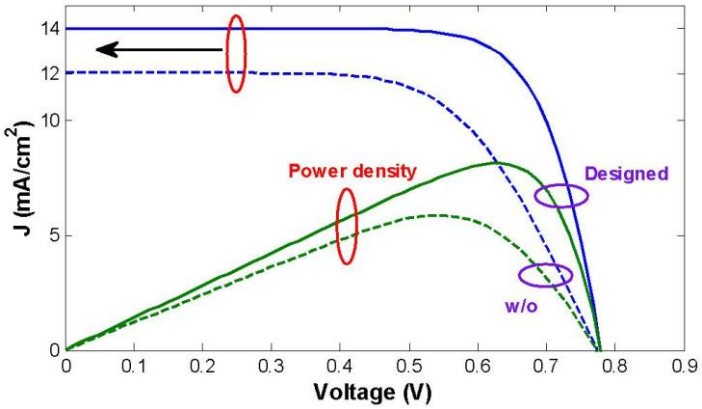

Fig. 5. IV characteristics of the solar cells without and with plasmonic design. The considered optimal plasmonic design is: R_M = 80 nm and Λ = 400 nm. The corresponding V-dependent output power densities are plotted as well in the same figure. The solar cell operating parameters can be easily obtained from the information provided by the IV curve.

Table 1. Performance comparison of the thin-film GaAs solar cells before and after incorporating the optimized plasmonic design.

	J_{sc} (mA/cm2)	V_{oc} (V)	P_{max} (mW/cm^2)	FF (%)	η (%)
Before design	12.06	0.7724	5.864	63.0	6.1
After design	14.00	0.7793	8.128	74.5	8.5

Enhancement ratio	16.1%	1%	38.6%	18.3%	39.3%

3 Experimental work

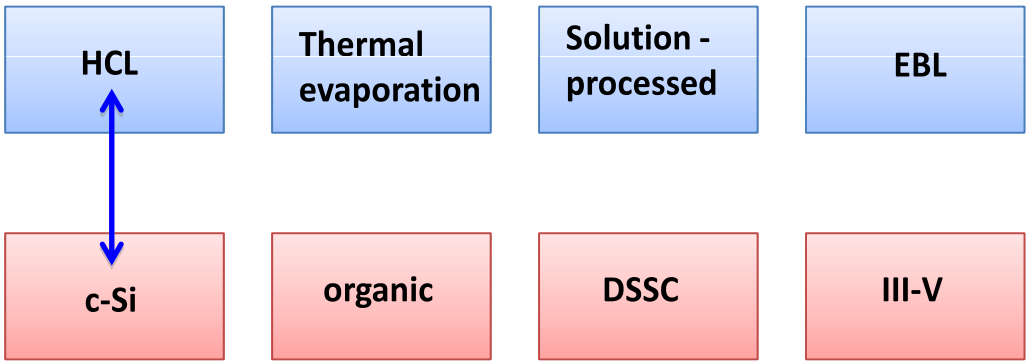

This section is concerned with experimental work on Si based plasmonic solar cells fabricated using hole-mask colloidal lithography.

3.1 Experimental systems for broadband performance enhancements

Experimental systems have so far aimed at Si solar cells. Ag nanodisks were fabricated on silicon wafers with a thin layer of SiO_2 as spacer using hole-mask colloidal lithography. The Ag disks have a height of 50 nm and diameters of 80 nm, 100 nm and 200 nm, respectively. As a test of broadband performance, nanodisks of mixed diameters 60, 80, 100 and 200 nm were also made. On the top of all the samples, a film of 65 nm SiO_2 was deposited, serving both as a capping layer preventing oxidation of Ag disks and as an anti-reflection layer. A typical SEM image of the samples with 100 nm Ag disks is shown in Fig. 6.

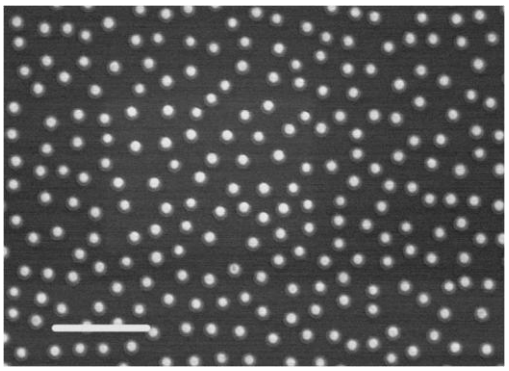

Fig. 6. SEM image of Ag nanodisks of 100 nm diameter on Si with 10 nm SiO_2 spacer and 65 nm SiO_2 as capping layer. Scale bar: 1 μm

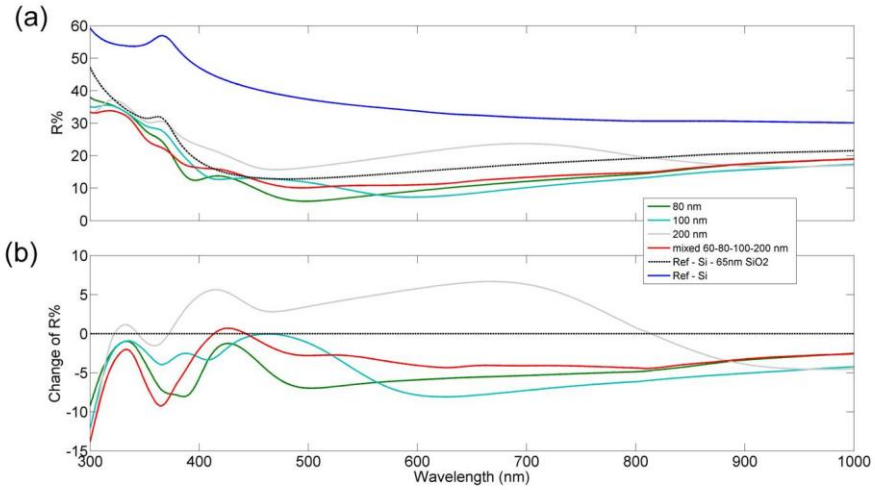

Fig. 7. (a) Reflection spectra of Ag nanodisks on Si with 10nm spacer and 65nm capping layer. The diameters are 80 nm, 100 nm, 200 nm and a mix of 60, 80, 100 and 200 nm, respectively. (b) Change of reflectance of samples with Ag disks compared to the reference Si sample with 65 nm SiO_2 coating.

Reflection spectra of the samples with various Ag disks diameters were measured using a Cary 5000 spectrophotometer with specular reflection accessory, and are shown in Figure 7(a). The spectra of silicon with (black curve) and without (blue curve) a SiO_2 capping layer are also given as references. It is seen that with 200 nm disks (gray curve), the reflectance is significantly higher than the reference sample with SiO_2 capping layer almost over the whole spectral range, indicating that it is obviously not a candidate for efficiency enhancement in a front-mode configuration. However, one should note that in the back-mode configuration where the red light is expected to be preferentially reflected at the back side, Ag nanodisks of size 200 nm could then be a good choice. The tests will be carried out on the coming batch of multi-crystalline Si samples from IMEC. However, the samples with 80nm, 100nm and mixed sizes Ag disks show a general decrease of reflectance, meaning the enhancement of light trapping. The change of reflectance is given in Figure 7(b). The decrease of total reflectance integrated over 300nm-1000nm compared to the reference is ~24.5%, ~25.1% and ~18.5% for Ag nanodisks of 80nm, 100nm and mixed sizes, respectively. The next step will be to fabricate similar structures with diameter 100 nm and mixed sizes on epitaxial Si solar cells with different thickness of active layers for solar cells performance test.

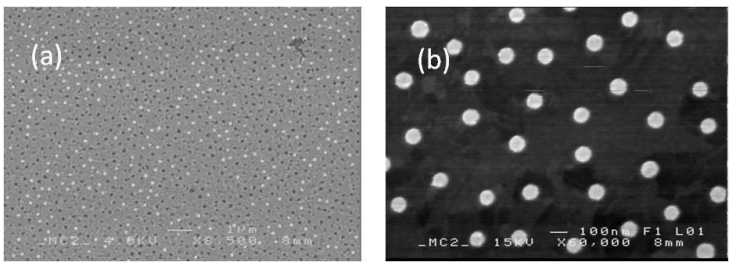

Fig. 8. SEM image of Ag nanodisks on Ag film (a) and Au nanodisks on Au film structures (b).

Following the geometry of broadband plasmonic arrays with reflective support proposed in Deliverable 1.1, disks-over-film systems were also tested. Ag disks on Ag film separated by a thin spacer turned out to be problematic in colloidal lithographic fabrication (see SEM image in Fig. 8 (a)). The Ag film was partially removed together with the top Ag nanodisks during liftoff, perhaps due to the weak stiffness of

Ag film. However, as an alternative, Au disks on Au film separated by Al_2O_3 layer were successfully fabricated (Fig. 8 (b)).

Figure 9 gives the optical characterization results of Au nanodisks on Au film structures with various thickness of Al_2O_3 spacer layer. The diameter and height of Au disks are 110 nm and 50 nm, respectively. As seen in Figure 9 (a), by decreasing the thickness of Al_2O_3 layer, the nanodisks on glass substrates exhibit a slight redshift of resonance due to the substrate effect – the coupling between the nanodisks and their images in the substrate. However, if the nanodisks are on Au film, a dramatic redshift is observed accompanied by prominent peak broadening, resulted from the plasmonic hybridization between the nanodisks and the Au film (Figure 9 (b)). Together with the spectral results at oblique incidence of 45 degrees shown in Figure 9 (c) and 9 (d), it indicates that the disks-over-film system is ideal for broadband plasmonic solar cells working in the back-reflection mode where the wavelength to be reflected can be finely tuned by adjusting the thickness of the spacer.

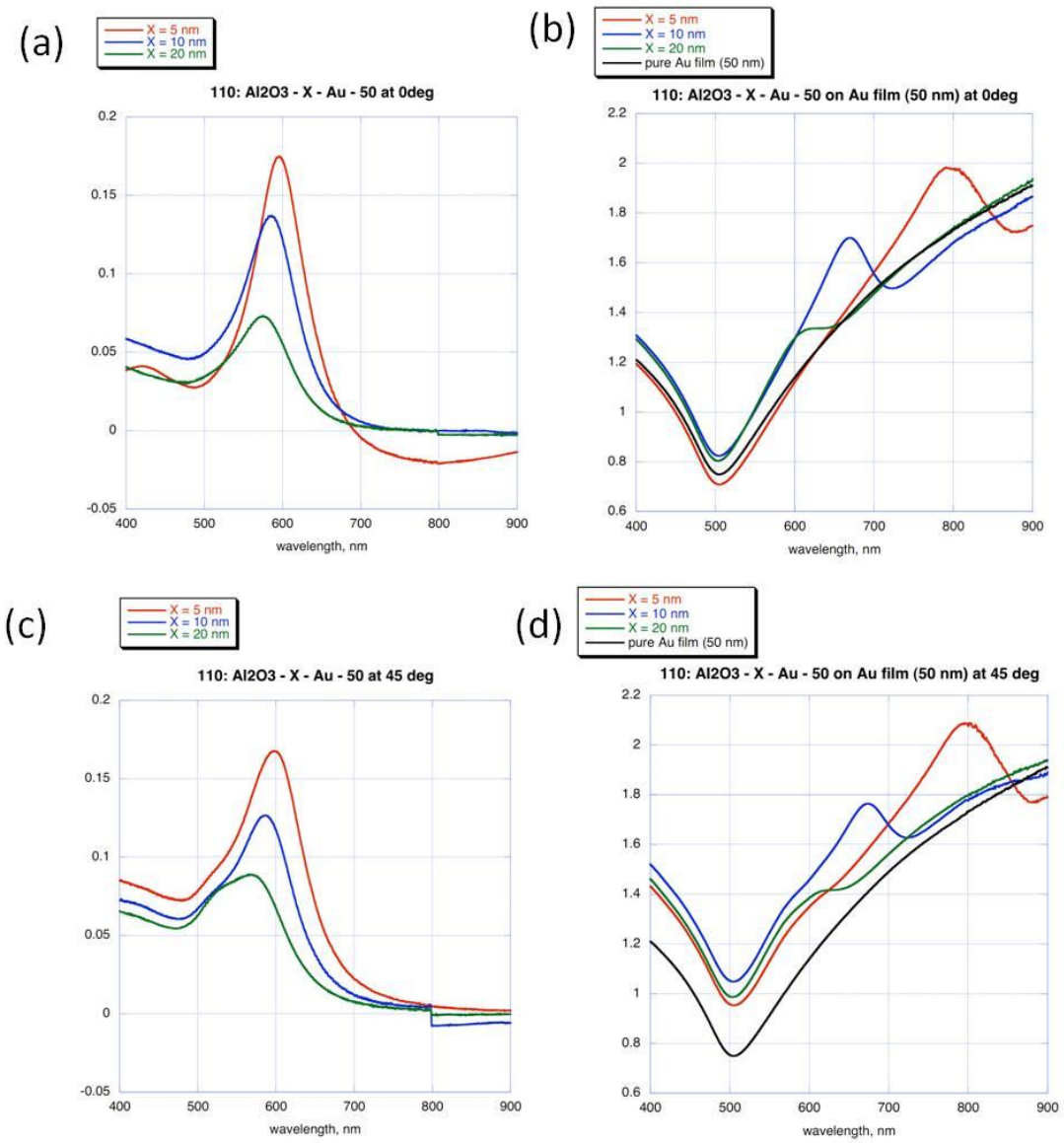

Fig. 9. Extinction spectra of Au nanodisks (100 nm in diameter and 50 nm in height) on glass and on 50 nm Au film with various thickness of Al_2O_3 spacer layer. (a) On glass at normal incidence. (b) On 50 nm Au film at normal incidence. (c) On glass at 45 degrees incidence. (d) On 50 nm Au film at 45 degrees incidence.

4 Conclusions

In section 2 a Comsol-based 3D model was developed in order to realize a robust simulation of plasmonic solar cells. This model conducts the electromagnetic calculation to obtain the field (power) distribution in the device under solar light injection and includes the effect of plasmonic structures. The electron and hole transport in the device are simulated by an electric calculation in the model, which calculates the dark current and the frequency-dependent photocurrents. Based on the optical and electric responses obtained from the 3D simulation, rich information of plasmonic solar cells can be achieved, which provide a better evaluation for the designed plasmonic solar cells.
The validity of the model has been verified through good agreement with the experiments of GaAs solar cells in both conventional and thin-film configurations from the literature. A further simulation on the optically thin GaAs plasmonic solar cells confirmed the possibility of using plasmonic nanostructures to improve the performance of solar cells. Silver nanoparticles with radius of 80 nm and spacing of 400 nm were suggested as the optimum plasmonic design for the thin-film solar cell considered here. It was also shown that the photocurrent, maximum output power and light-conversion efficiency can be improved by 16.1%, 38.6% and 39.3%, respectively, after introducing the optimally designed plasmonic nanostructures.
In section 3 the optical properties of nanodisk and nanodisk-on-film structures (for use on the front and rear of solar cells, respectively) were investigated experimentally. The results demonstrated broadband improvements in terms of light trapping in the solar cell and in terms of light scattered back into the absorbing layer from the rear surface.

5 References

[1] S. P. Tobin, S. M. Vernon, C. Bajgar, S. J. Wojtczuk, M. R. Melloch, A. Keshavarzi, T. B. Stellwag, S. Venkatensan, M. S. Lundstrom, and K. A. Emery, "Assessment of MOCVD- and MBE-grown GaAs for high-efficiency solar cell applications," *IEEE T. Electron. Dev.*, **37**(2):469-477, 1990.

[2] S. P. Tobin, S. M. Vernon, C. Bajgar, L. M. Geoffroy, C. J. Keavney, M. M. Sanfacon, and V. E. Haven, "Device processing and analysis of high efficiency GaAs cells," *Solar Cells*, **24**:103-115, 1988.

[3] S. P. Tobin, S. M. Vernon, S. J. Wojtczuk, C. Bajgar, M. M. Sanfacon, and T. M. Dixon, "Advances in high-efficiency GaAs solar cells," *Photovoltaic Specialists Conf.*, **1**:158-162, 1990.

[4] K. Nakayama, K. Tanabe, and H. A. Atwater, "Plasmonic nanoparticle enhanced light absorption in GaAs solar cells," *Appl. Phys. Lett.*, **93**:121904, 2008.